FAST ISAR IMAGE SIMULATION OF TARGETS AT ARBITRARY ASPECT ANGLES USING A NOVEL SBR METHOD

X. Y. He, X. B. Wang, X. Y. Zhou, B. Zhao, and T. J. Cui

State Key Laboratory of Millimeter Waves
School of Information Science and Engineering
Southeast University, Nanjing 210096, China

Abstract—We present an efficient way to generate the inverse synthetic aperture radar (ISAR) image of a target at an arbitrary aspect angle using the shooting and bouncing ray (SBR) method, which is much faster than the conventional approach by inverse Fourier transforming the computed scattered fields over frequency and aspect domain. We propose a general image-domain ray-tube integration formula, which contains aspect-dependent factors. The new formula can provide ISAR images of a target rapidly and conveniently in different image planes at different aspect angles in a world coordinate system. The ISAR images of a cube and an aircraft for several aspect angles and different image planes are presented to demonstrate the efficiency and accuracy of the general formula. The proposed method is more significant when large amount of ISAR images of a target are required to build the database for target recognition.

1. INTRODUCTION

The synthetic aperture radar (SAR) or inverse synthetic aperture radar (ISAR) based automatic target recognition (ATR) have become increasingly popular due to their ability to work under almost all weather conditions and complicated environment [10, 11, 22]. The SAR synthetically increases the antenna's size or aperture to increase the image resolution. With the radar moving on the platform, a pulse is transmitted at multiple positions. The return echoes pass through the receiver and are recorded in an echo store, yielding an effective increase

of the antenna aperture. Similarly, ISAR is used to generate images of a moving target. The concept and processing algorithms are similar to SAR, but it is the movement of the target, not the radar system, that is used to effectively increase the aperture of the radar's antenna. The subject of SAR and ISAR has been of great interest and a wide range of research has been carried out on different issues [3–5, 12–14, 23, 24].

SAR and ISAR images are powerful visualization tools that can provide high-resolution two-dimensional (2D) electromagnetic (EM) images of an area or a target of interest. Usually the SAR or ISAR images are obtained by coherently signal processing the received radar echoes of transmitted pulses. A high resolution in the range direction is achieved by the large bandwidth of the transmitted impulses, while a high resolution in the cross-range direction is obtained by the synthetic aperture generated by motion of the target or possibly by motion of the radar platform. When the target or radar moves, usually in an unknown trajectory, the motion compensation is considered in the image formation [14, 17, 19]. ATR based on SAR or ISAR images has great importance on the target recognition, but its development is still slow due to the lack of valid SAR/ISAR image database, which was merely obtained by measurements previously.

The fusion of computer graphics and modern computational electromagnetics has facilitated a possible access for the necessary database of SAR and ISAR images [4–9, 20–24]. Since the movement of target or radar is equivalent to that radar receives echoes at different aspect angles, the SAR and ISAR images of a given target can be simulated using the scattered fields over a frequency band and a range of aspect angles. Hence, in the means of simulation, there is no difference between SAR and ISAR images. Because what we studied in this paper is aircraft, the moving target, we adopt the term of ISAR image. Combining the measured and simulated SAR and ISAR images together, a large database could be set up, which will enhance the progress of ATR.

In recent years, the ISAR imaging with the EM model has been well studied [4–9, 20, 24]. In the conventional ISAR-image formation, the target is located in the center of the coordinate system, and the scattered fields are computed over a band of frequencies which determines the range resolution and a band of angles which determines the cross-range resolution. The ISAR image of target on the given angle is derived by inverse Fourier transformation of the 2D data [1, 2]. In [3], three different image-formation approaches were compared and the images were obtained respectively. In [4], the ISAR image was achieved based on the full-wave numerical technique, the finite difference time domain method, which can avoid evaluating the multi-

scattering effects on the image. In [5], the shooting and bouncing rays (SBR) method was used to calculate the scattered fields, and then the ISAR image was obtained through the inverse Fourier transform.

In the above methods, however, the whole computation procedure has to be carried out over a band of frequencies and a band of aspect angles to get the scattered data. Hence it is rather time consuming to obtain high resolution images of a complicated target. A significant contribution was the introduction of SBR method to the ISAR-image formation [6], which is under the concept of the equivalence between the bistatic and monostatic radar cross sections (RCSs) in a small angle approximation [7, 16]. This procedure can briefly be described by the following formula [6]

$$O(x, y) = \sum_{i=1}^{N} O_i(x, y) \tag{1}$$

where, $O_i(x, y)$ is the contribution of each effective ray tube to the ISAR image which has a closed form under the small angle approximation, and N is the number of effective ray tubes. Using such a technique, the ISAR image can be accessed without the laborious multiple frequency-aspect calculations. In this paper, we propose an efficient way to generate the ISAR images of a target at an arbitrary aspect angle using the SBR method. We derive a general formula which contains the aspect dependent factors, and then write it in a convolution form and use the fast Fourier transform to carry out the convolution, the scheme can get a speed gain of a factor of more then two hundred. The proposed method is more significant when large amount of ISAR images of a target are required to build the database for ATR.

2. GENERAL FORMULA

The SBR method is a high-frequency EM simulation technique to compute the scattering properties of arbitrary shaped realistic targets, which becomes more powerful when combined with the computer graphics since arbitrary-shaped targets can be modeled accurately [8, 9, 16]. In the SBR method, the ray path and the geometrical physics (GO) field associated with each ray are considered respectively. For a specific ray, when it is intersected with the target, the reflected ray direction will be determined by the Snell's law, where the normal vector is known. The GO field can be obtained by determining two coefficients: the reflection coefficients and the divergence factor. By using the reflected ray as the incident ray, the

above procedure can be repeated until the ray escapes the target. For conducting object, the physical optics (PO) integration is carried out at the wave front of the ray tube just before the ray escapes the target.

Millions of rays modeling the incident plane wave are launched towards the target. The total scattered field at an observation point is the summation of the contributions from each ray tube. The SBR technique is more efficient especially when multiple bouncing rays contribute to the scattered field. To derive the general ISAR image formula at an arbitrary aspect angle, we consider the ray-tube integration formula which calculates the far-field scattered electric field at an arbitrary observation point (r, θ, φ) [9]

$$\mathbf{E}(r, \theta, \varphi) = \frac{e^{-jkr}}{r} \left(\hat{\theta} A_\theta + \hat{\varphi} A_\varphi \right) \tag{2}$$

where A_θ and A_φ are related to the aperture field of the ray tube by the surface integral based on the Huygens' principle. By carrying the integral over the wave front of the ray, we get the approximate formula for A_θ and A_φ as

$$\begin{bmatrix} A_\theta \\ A_\varphi \end{bmatrix} = \sum_{i=1}^{N} \begin{bmatrix} B_\theta \\ B_\varphi \end{bmatrix} \left(\frac{jk}{2\pi} \right) (\Delta A)_{\text{exit}} S(\theta, \varphi) e^{j\hat{k} \cdot \mathbf{r}_A}$$

$$B_\theta = -s_1 E_3 \cos \varphi - s_2 E_3 \sin \varphi + s_3 (E_1 \cos \varphi + E_2 \sin \varphi)$$

$$B_\varphi = s_1 (E_3 \cos \theta \sin \varphi + \sin \theta E_2) + s_2 (-E_1 \sin \theta -$$
$$E_3 \cos \theta \cos \varphi) + s_3 (E_2 \cos \theta \cos \varphi - E_1 \cos \theta \sin \varphi)$$

in which N is the total number of the effective ray tubes, $\mathbf{r}_A$ is the position vector of the last hit point on the target, $S(\theta, \varphi)$ is the shape function [15] and can be usually assumed unity if the ray tube area is sufficiently small, and $(\Delta A)_{\text{exit}}$ is the cross section of the exit ray tube at point A. $\mathbf{E}(A) = E_1 \hat{x} + E_2 \hat{y} + E_3 \hat{z}$ is the electric field with each ray tube at A, $\mathbf{s} = s_1 \hat{x} + s_2 \hat{y} + s_3 \hat{z}$ is the exit ray tube direction, and $\mathbf{k} = k_x \hat{x} + k_y \hat{y} + k_z \hat{z} = k \hat{k}$ is the observation wave vector.

The ISAR image of a target can be generated through a 2D Fourier transform

$$O_{\theta, \varphi}(x, z) = \frac{1}{(2\pi)^2} \iint_{-\infty}^{\infty} \widetilde{O}_{\theta, \varphi}(k_x, k_z) e^{-j(k_x x + k_z z)} dk_x dk_z \tag{3}$$

where

$$\widetilde{O}_{\theta, \varphi}(k_x, k_z) = \frac{4\pi r}{-jkE_0 e^{-jkr}} E_{\theta, \varphi}^s(k, \theta, \varphi)$$

and $E_{\theta, \varphi}^s(k, \theta, \varphi)$ is the far-field scattered electric field. The subscript θ or φ donates the corresponding polarization. In a global coordinate system, the target is located at the origin. We set the image plane as

the x-z plane and the incident wave as the z direction for convenience. The bistatic observation angle varies from $-\theta_0$ to θ_0 and the frequency from $k_{\min}$ to $k_{\max}$ to achieve the Fourier space information. Under the small angle condition we get the approximate expression of the contribution of each effective ray tube to the ISAR image

$$
\begin{aligned}
O_{\theta,\varphi}(x,z) &= -\frac{k_0}{\pi^2} \sum_{i=1}^{N} \left\{ (\Delta A)_{\text{exit}_i} \cdot \int_{k_{\min}}^{k_{\max}} e^{-jk(2z+d_i-z_i)} dk \right. \\
&\left. \cdot \int_{-\theta_0}^{\theta_0} (\alpha_i + \theta\beta_i) e^{-jk_0(2z+d_i-z_i)} d\theta \right\}
\end{aligned}
\tag{4}
$$

The integrations can be easily carried out analytically. After ignoring the terms of order θ_0^2, we get the closed form expression as

$$
\begin{aligned}
O_{\theta,\varphi}(x,z) &= -\frac{k_0}{\pi^2} \sum_{i=1}^{N} \left\{ (\Delta A)_{\text{exit}_i} \cdot \Delta k e^{-jk_0(2z+d_i-z_i)} \right. \\
&\left. \cdot\text{sinc}\left[\Delta k \left(z + \frac{d_i - z_i}{2}\right)\right] \cdot 2\alpha_i\theta_0\text{sinc}[k_0\theta_0(x - x_i)] \right\}
\end{aligned}
\tag{5}
$$

in which $\text{sinc}(u) = \sin u/u$, $\text{sinc}'(u) = (-\text{sinc}(u) + \cos u)/u$, k_0 is the center wave number, $\Delta k = k_{\max} - k_{\min}$, d_i is the distance traveled by the ith ray tube, (x_i, z_i) is the position of the last hit point on the target, and α_i is the GO field associated with the ith ray. We call the position dependent part of every ray tube

$$
\begin{aligned}
h\left(x - x_i, z' - d_i{}'\right) &= \Delta k e^{j2k_0(z'-d_i{}')}\text{sinc}\left[\Delta k \left(z' - d_i{}'\right)\right] \\
&\cdot 2\alpha_i\theta_0\text{sinc}\left[k_0\theta_0(x - x_i)\right]
\end{aligned}
\tag{6}
$$

as the ray spread function, where $z' = -z$ is defined as the range direction, $d_i{}' = (d_i - z_i)/2$ is half of the distance traveled by the ith effective ray tube. The ray spread function obtain its maximum at $z' = (d_i - z_i)/2$ in the range direction, and $x = x_i$ in the cross-range direction which is the last hit-point on the target.

In order to obtain the ISAR image of a target at arbitrarily continuous aspect angles, we present a general formula, in which the aspect-dependent factors in (5) need to be modified. When the ISAR image of an arbitrary aspect angle is considered, the range direction is along the incident direction, and the cross-range direction is orthogonal to the range direction and within the aspect-scanning plane. Similarly, the image space along the range direction and cross-range direction are updated by the aspect-dependent ray spread function, whose peak position is determined according to each ray tube. Analogically, we

get a general formula and the contribution of each effective ray tube to the arbitrary-aspect ISAR image is described as

$$O_{\theta,\varphi}(R, CR) =$$

$$-\frac{k_0}{\pi^2} \sum_{i=1}^{N} \left\{ (\Delta A)_{\text{exit}_i} \cdot \left\{ \Delta k e^{jk_0\left(R - \frac{d_i - \hat{k} \cdot \mathbf{r}_A}{2}\right)} \text{sinc}\left[\Delta k \left(R - \frac{d_i - \hat{k} \cdot \mathbf{r}_A}{2} \right) \right] \right\} \right.$$

$$\cdot \left. \left\{ 2\alpha_i \theta_0 \text{sinc}\left[k_0 \theta_0 \left(CR - \hat{k}_\perp \cdot \mathbf{r}_A \right) \right] \right\} \right\} \tag{7}$$

where $\hat{k}$ is the range direction, $\hat{k}_\perp$ is the cross-range direction, and the two directions determine the image plane. R and CR are the coordinates in the two directions respectively. The above equation is a general formula, from which ISAR images in different directions and different image planes can be obtained rapidly and conveniently. This is significantly important to the setup of ISAR image database for the ATR usage.

The imaging formula (5) is obtained by the Fourier transform of the k-space data (3) analytically. The process has already fulfilled the broadband property in the pulse radar (corresponding to the range domain) and the relative motion between radar and target (corresponding to the cross-range domain). Hence, the ISAR image is formed in the image-domain directly without using the Fourier transform numerically. We find that each ray tube contributes to the ISAR image in a form of conduct of two sinc functions. The image plane is updated by each ray tube. The amplitude and the position of each sinc function depend on the cross section of ray tube, the range direction and coordinate, the cross-range direction and coordinate, the GO field at the last point, the coordinates of the last hit point on the target, and the traveling distance. Using the general formula (7), the ISAR images of a target in any image planes and at arbitrary aspect angles can be obtained rapidly without rotating the target model.

3. FAST-IMPLEMENTATION SCHEME

The general formula (7) can be recognized as a convolution form

$$O_{\theta,\varphi}(CR, R)$$

$$= -\frac{k_0}{\pi^2} \cdot \left\{ \sum_{i=1}^{N} (\Delta A)_{\text{exit}_i} \alpha_i \delta(R - R_i, CR - CR_i) \right\} * h(R, CR), \tag{8}$$

where $R_i = (d_i - \hat{k} \cdot \mathbf{r}_A)/2$, $CR_i = \hat{k}_\perp \cdot \mathbf{r}_A$, and $x(R, CR) = \sum_{i=1}^{N} (\Delta A)_{\text{exit}_i} \alpha_i \delta(R - R_i, CR - CR_i)$ is a two-dimensional unequal

spaced discrete array. The ray spread function $h(R, CR)$ is defined in (6). We apply a linear interpolation method to make an equally spaced array $x'(R, CR)$ after the ray tracing. Then following fast scheme is available:

$$O_{\theta,\varphi}(CR, R)$$
$$= -\frac{k_0}{\pi^2} \cdot \textbf{IFFT2D}\Big\{\textbf{FFT2D}\big[x'(R, CR)\big] \cdot \textbf{FFT2D}\big[h(R, CR)\big]\Big\}. \quad (9)$$

Using the two-dimensional FFT algorithm, the computation time would be reduced immensely, as shown in Table 1.

4. NUMERICAL RESULTS

Several numerical results are presented to demonstrate the validity and accuracy of the proposed method. The ISAR images generated using this general image-domain formula are compared to those generated using the conventional Fourier transforming method. We will show a simple target of cube first, and then a complex aircraft P51.

First, we consider the ISAR image of a cube with the size of $10\,\text{m} \times 10\,\text{m} \times 10\,\text{m}$, whose geometrical model is shown in Fig. 1. The incident direction is $\theta = 90°$ and $\varphi = 45°$, and the image plane is the x-y plane. The central frequency is $3\,\text{GHz}$ and the bandwidth is $1\,\text{GHz}$. Hence, the range resolution is $0.15\,\text{m}$. The cross-range resolution is also set as $0.15\,\text{m}$ for observation convenience, while it is dependent on the width of observation angle. In order to achieve the cross-range resolution, the bistatic observation angle is set around the incident direction over a range of $\pm 19.1°$. The range window and the cross-range window are both set as $[-L/2, L/2]$, where L is chosen
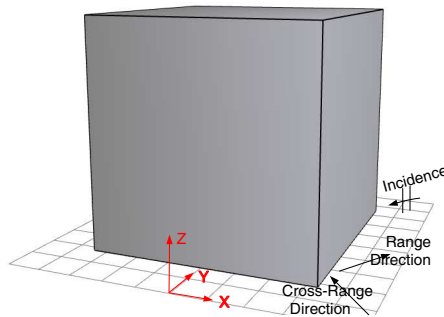
Figure 1. The geometrical model of a cube target.

to be twice the size of the target. The ISAR image is computed on a 256×256 grid, and the result is shown in Fig. 2(b).

A numerical result of the same target on the equal condition using the conventional frequency-aspect method is presented in Fig. 2(a) to demonstrate the accuracy and computational time of the general formula we derived. The monostatic observation angle over a range of $\pm 9.55°$ around the incident direction is set for the reason of monostatic and bistatic equivalence [2, 7]. From Fig. 2, we clearly notice the strong scattering centers in the two ISAR images, which are corresponding to the three corners. The comparison of the computational time is shown in Table 1.

Figure 3 is the geometrical model of the aircraft P51. The target model consists of 2600 planar triangular facets and it is encircled by a box of $14.115\,\text{m} \times 16.984\,\text{m} \times 4.499\,\text{m}$. Figs. 4 and 5 show the 2D ISAR images of the P51 aircraft, where the incident direction is
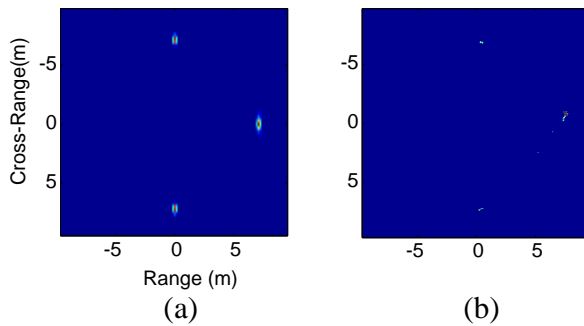
Figure 2. The ISAR images of the cube, in which the incident direction is chosen as $\theta = 90°$ and $\varphi = 45°$, and the resolution is $0.15\,\text{m}$. (a) Conventional approach by inverse Fourier transforming the computed scattered fields over the frequency-aspect domain. (b) General image-domain ray-tube integration formula.
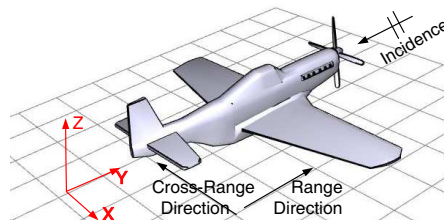
Figure 3. The geometrical model of an P51 aircraft target.

Table 1. Comparison of the computational time to generate the ISAR images using the two methods.

	Cube (sec)	P51 (sec)
Conventional Method	115	15700
Generate Formula	10	74
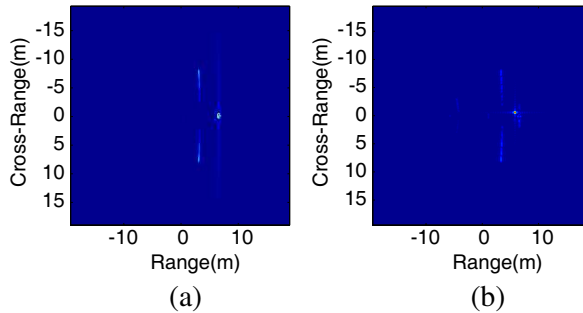
Figure 4. The 2D ISAR images of the P51 aircraft target in the x-y plane, in which the incident direction is chosen as $\theta = 90°$ and $\varphi = 0°$, and the resolution is set as $0.3\,\mathrm{m}$. (a) The ISAR image generated by the conventional method. (b) The ISAR image generated from the new formula.
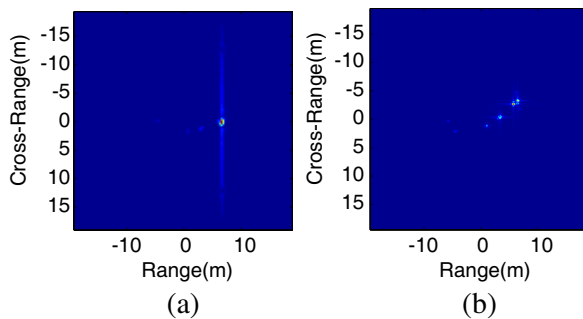
Figure 5. The 2D ISAR images of the P51 aircraft target in the x-z plane, in which the incident direction is chosen as $\theta = 90°$ and $\varphi = 0°$, and the resolution is set as $0.3\,\mathrm{m}$. (a) The ISAR image generated by the conventional method. (b) The ISAR image generated from the new formula.

$\theta = 90°$ and $\varphi = 0°$. The x-y plane is selected as the image plane in Figs. 4(a) and 4(b), and the x-z plane in Figs. 5(a) and 5(b). In the conventional method, the scattered fields are computed in a frequency

range from $2.5\,\mathrm{GHz}$ to $3.5\,\mathrm{GHz}$ in 300 steps and in an azimuth angle range from $-9.55°$ to $9.55°$ in 300 steps, and the imaging result is shown in Fig. 4(a). The ISAR image generated from the general formula on a 512×512 grid is shown in Fig. 4(b), where the same frequency range is used with a bistatic angle window of $\pm 19.1°$. Under the same frequency band, when the elevation angle ranges from $80.45°$ to $99.55°$ in 256 steps, the ISAR image from the conventional method is shown in Fig. 5(a). Correspondingly, the ISAR image from the general formula on a 512×512 grid is shown in Fig. 5(b), where the window of bistatic
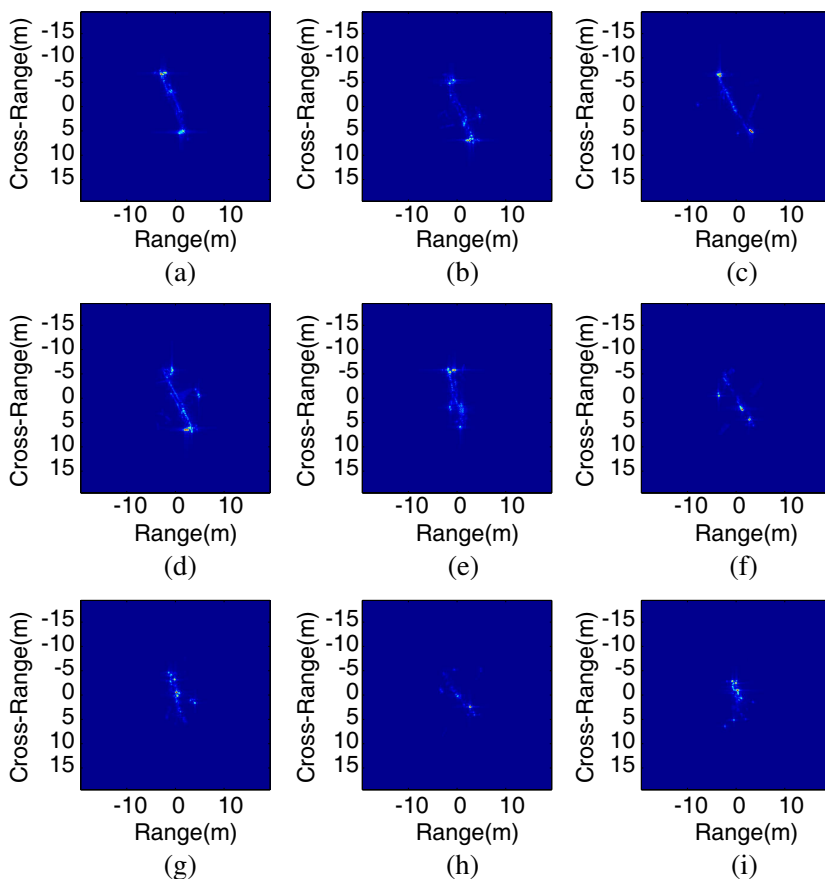
Figure 6. The 2D ISAR images of the P51 aircraft generated from the new formula, in which the incident elevation angle is $75°$, and the incident azimuth angle is from $33°$ to $57°$ with an incremental of $3°$, respectively, from (a) to (i). Here, the resolution is set as $0.3\,\mathrm{m}$.

angles is $\pm 19.1°$. Comparing Figs. 4(a) with 4(b) and 5(a) with 5(b), we notice that the dominating strong scattering centers have emerged in both the two method and the image generated by the new method has been better focused.

Moreover, the computation time of generating a ISAR image with the proposed method in this paper is much smaller than the conventional method, as shown in Table 1. Where the computation time of the conventional method is the sum of the SBR method to create the scattered fields and the image creation process. There is a speed gain of a factor of more than two hundred. All computations are performed in a personal computer (HP Compaq dc7800). There are two factors which give rise to the superior speed performance of the new imaging formation over the conventional approach. First, the bistatic approximation and the time-domain integral allow the ray tracing to be performed only one time. Second, the using of FFT accelerated the imaging process.

The proposed method is more significant when large amount of ISAR images are required to build the database for ATR, where ISAR images for different aspect angles and different image planes are needed. In Fig. 6, the ISAR images of the P51 aircraft for different azimuth angles are given, in which the frequency is the same as that in the earlier example, the incident elevation angle is $75°$, and the azimuth angle is from $33°$ to $57°$ with an incremental of $3°$. Without rotating and adjusting the target model, the ISAR images are generated rapidly and conveniently, as shown in Fig. 6.

5. CONCLUSION

In this paper, we proposed an efficient way to generate the ISAR images of a target at an arbitrary aspect angle using the SBR method. We derived a general formula containing the aspect-dependent factors, which can provide ISAR images of a target rapidly and conveniently in different image planes at different aspect angles in a world coordinate system, without scanning the frequencies and aspect angles. As the general formula can be written in a convolution form, the FFT method is used to accelerate the convolution after a linear interpolation. The proposed method is more significant when large amount of ISAR images of a target are required to build the database for ATR.

We remark that the image-domain ray-tube integration formula based on the SBR technique is inefficient to take into account the multiple scattering effects. When high fidelity ISAR images are required, especially for stealth radar targets, the effects of edge diffraction are non-negligible. Hence the contribution of the edge

diffraction to the ISAR images must be considered. Moreover, the current ISAR simulation is only restricted to conducting objects. The image calculation of large objects including dielectric components is still difficult.

As the millimeter-wave radars have been common these days, the high-frequency approximations will become more applicable. Furthermore, for the aim of producing a library (i.e., large volume) of images for the ATR purpose, and for the real-time imaging purpose, the proposed method is very significant.

REFERENCES

1. Farhat, N. H., C. L. Werner, and T. H. Chu, "Prospects of three-dimensional projective and tomographic imaging radar networks," *Radio Sci.*, Vol. 19, 1347–1355, 1984.

2. Carrara, W. G., R. S. Goodman, and R. M. Majewski, *Spotlight Synthetic Aperture Radar-signal Processing Algorithms*, Artech House, Boston, 1995.

3. Sasaki, K., M. Shimizu, Y. Watanabe, and E. Pottier, "New method in ISAR image reconstruction," *Proceeding of CIE International Conference on Radar*, Oct. 662–664, 2001.

4. Gu, X., Y. H. Zhang, and X. K. Zhang, "Electromagnetic simulation of ISAR imaging with supper-resolution," *Proceeding of 1st Asian and Pacific Conference on Synthetic Aperture Radar*, 595–598, Nov. 2007.

5. Wen, X. Y., C. Wang, and H. Zhang, "Complex object's ISAR image simulation," *Proceedings of 2005 IEEE International Symposium on Geoscience and Remote Sensing*, Vol. 5, 3181–3183, Jul. 2005.

6. Bhalla, R. and H. Ling, "Image-domain ray-tube integration formula for the shooting and bouncing ray technique," *Radio Sci.*, Vol. 30, 1435–1446, Sep./Oct. 1995.

7. Bhalla, R. and H. Ling, "ISAR image formation using bistatic computed from shooting and bouncing ray technique," *Journal of Electromagnetic Waves and Applications*, Vol. 7, No. 9, 1271–1287, Sep./Oct. 1993.

8. Ling, H., C. R. Hou, and S. W. Lee, "Shooting and bouncing rays: Calculating the RCS of an arbitrary shaped cavity," *IEEE Trans. Antennas Propagat.*, Vol. 37, 194–205, Feb. 1989.

9. Lee, S. W., H. Ling, and R. Chou, "Ray tube integration in shooting and bouncing ray method," *Microwave Opt. Tech. Lett.*, Vol. 1, 286–289, Oct. 1988.

10. Novak, L. M., G. J. Owrika, W. S. Brower, and A. L. Weaver, "The automatic target recognition system in SAIP," *The Lincoln Laboratory Journal*, Vol. 10, No. 2, 187–202, 1997.

11. Toussaint, J. A. and D. M. Martinsek, "Integrated precision SAR targeting: A SAR targeting simulation," *IEEE Transactions on Aerospace and Electronic Systems*, Vol. 14, 29–32, Feb. 1999.

12. Hinz, S., F. Meyer, M. Eineder, and R. Bamler, "Traffic monitoring with spaceborne SAR-Theory, simulations, and experiments," *Computer Vision and Image Understanding*, Vol. 106, 231–244, 2007.

13. Van den Broek, B., T. Bieker, and L. Ewijk, "Comparison of modelled to measured high-resolution ISAR data," *MMW Advanced Target Recognition and Identification Experiment*, 17, 2005.

14. Moreira, A. and Y. Huang, "Airborne SAR processing of highly squinted data using a chirp scaling approach with integrated motion compensation," *IEEE Transactions on Geoscience and Remote Sensing*, Vol. 32, No. 5, 1029–1040, Sep. 1994.

15. Lee, S. W. and R. Mittra, "Fourier transformation of polygonal shape function and its application in electromagnetics," *IEEE Trans. Antennas Propagat.*, Vol. 31, 99–103, 1983.

16. Buddendick, H. and T. F. Eibert, "Concept for accelerated ray-based monostatic RCS simulations using bistatic approximations," *Adv. Radio Sci.*, Vol. 7, 29–35, 2009.

17. Chen, V. C. and W. J. Miceli, "Simulation of ISAR imaging of moving targets," *IEE Proceedings Radar, Sonar and Navigation*, Vol. 148, 160–166, Jun. 2001.

18. Hagelen, M., A. Wahlen, and T. Brehm, "ISAR Imaging of flying helicopters at millimeter-wave frequencies," *First European Radar Conference 2004, EURAD*, 265–268, 2004.

19. Jain, A. and I. Patel, "SAR/ISAR imaging of a nonuniformly rotating target," *IEEE Transactions on Aerospace and Electronic Systems*, Vol. 28, 317–321, Jan. 1992.

20. Garcia-Fernndez, A. F., J. Grajal, and O. A. Yeste-Ojeda, "Analysis of ISAR images of a helicopter by a facet model," *Proceedings of the 2008 International Conference on Radar*, Adelaide, 32–37, Sep. 2008.

21. Youssef, N. H., "Radar cross section of the complex target," *Proceedings of the IEEE*, Vol. 77, 722–734, May 1989.

22. Danklmayer, A., B. J. Doring, M. Schwerdt, and M. Chandra, "Assessment of atmospheric propagation effects in SAR images,"

IEEE Transactions on Geoscience and Remote Sensing, Vol. 47, No. 10, 3507–3518, 2009.

23. Vaupel, T. and T. F. Eibert, "Comparison and application of near-field ISAR-imaging techniques for far-field radar cross section determination," *IEEE Trans. Antennas Propagat.*, Vol. 54, No. 1, 144–151, Jan. 2006.

24. Vaupel, T. and F. Weinmann, "Validation of a 3-D near-field ISAR imaging technique with far-field RCS extraction by means of a hybrid GO-PO/PTD ray tracing algorithm," *3rd European Conference on EuCAP*, 691–695, 2009.